University of Wollongong

Research Online

Comparison of channelized hotelling and human observers in determining optimum OS-EM reconstruction parameters for myocardial SPECT

Karen L. Gilland
Johns Hopkins Medical Institutes

Benjamin M. W Tsui
Johns Hopkins Medical Institutes, btsui@jhmi.edu

Yujin Qi
Johns Hopkins Medical Institutes, yujin@uow.edu.au

Grant T. Gullberg
E. O. Lawrence Berkeley National Laboratory

Comparison of channelized hotelling and human observers in determining optimum OS-EM reconstruction parameters for myocardial SPECT

Abstract

The performance of the Channelized Hotelling Observer (CHO) was compared to that of human observers for determining optimum parameters for the iterative OS-EM image reconstruction method for the task of defect detection in myocardial SPECT images. The optimum parameters were those that maximized defect detectability in the SPECT images. Low noise, parallel SPECT projection data, with and without an anterior, inferior or lateral LV wall defect, were simulated using the Monte Carlo method. Poisson noise was added to generate noisy realizations. Data were reconstructed using OS-EM at 1 & 4 subsets/ iteration and at 1, 3, 5, 7 & 9 iterations. Images were converted to 2D short-axis slices with integer pixel values. The CHO used 3 radially-symmetric, 2D channels, with varying levels of internal observer noise. For each parameter setting, 600 defect-present and 600 defect-absent image vectors were used to calculate the detectability index (dA). The human observers rated the likelihood that a defect was present in a specified location. For each parameter setting, the AUC was estimated from 48 defect-present and 48 defect-absent images. The combined human observer results showed the optimum parameter setting could be in the range 5-36 updates ([number of subsets]/iteration × number of iterations). The CHO results showed the optimum parameter setting to be 4-5 updates. The performance of the CHO was much more sensitive to the reconstruction parameter setting than was that of the human observers. The rankings of the CHO detectability values did not change with varying levels of internal noise.

Keywords

determining, channelized, optimum, os, em, reconstruction, parameters, myocardial, spect, hotelling, human, observers, comparison

Disciplines

Engineering | Science and Technology Studies

Publication Details

Comparison of Channelized Hotelling and Human Observers in Determining Optimum OS-EM Reconstruction Parameters for Myocardial SPECT

Karen L. Gilland, *Member, IEEE*, Benjamin M. W. Tsui, *Fellow, IEEE*, Yujin Qi, *Member, IEEE*, and Grant T. Gullberg, *Fellow, IEEE*

Abstract—**The performance of the Channelized Hotelling Observer (CHO) was compared to that of human observers for determining optimum parameters for the iterative OS-EM image reconstruction method for the task of defect detection in myocardial SPECT images. The optimum parameters were those that maximized defect detectability in the SPECT images. Low noise, parallel SPECT projection data, with and without an anterior, inferior or lateral LV wall defect, were simulated using the Monte Carlo method. Poisson noise was added to generate noisy realizations. Data were reconstructed using OS-EM at 1 & 4 subsets/iteration and at 1, 3, 5, 7 & 9 iterations. Images were converted to 2D short-axis slices with integer pixel values. The CHO used 3 radially-symmetric, 2D channels, with varying levels of internal observer noise. For each parameter setting, 600 defect-present and 600 defect-absent image vectors were used to calculate the detectability index (d_A). The human observers rated the likelihood that a defect was present in a specified location. For each parameter setting, the AUC was estimated from 48 defect-present and 48 defect-absent images. The combined human observer results showed the optimum parameter setting could be in the range 5–36 updates ([number of subsets]/iteration × number of iterations). The CHO results showed the optimum parameter setting to be 4–5 updates. The performance of the CHO was much more sensitive to the reconstruction parameter setting than was that of the human observers. The rankings of the CHO detectability values did not change with varying levels of internal noise.**

I. INTRODUCTION

IN SPECT imaging, to make a fair comparison among different imaging system geometries and collimator geometries, the reconstruction parameters must be separately optimized for each system being compared. The optimum reconstruction parameters for a detection task are generally assumed to be those which maximize an index of image quality such as the area under the ROC curve (AUC) [1] or the detectability index (d_A) [2],[3]. Because there are so many parameter values to test in determining the optimum parameter settings, numerical observers, such as the Channelized

Hotelling observer (CHO) [2]–[5], provide a more practical method for parameter optimization than human observer studies, provided the numerical observer can predict human observer performance. Previous studies have compared the performance of the CHO to human observers for tumor detection in ^{67}Ga SPECT imaging [6]–[8] and cardiac defect detection in ^{99m}Tc-sestamibi SPECT imaging [9]–[13]. The ^{67}Ga SPECT studies showed good agreement between the CHO and human observer performance; however, for the ^{99m}Tc-sestmibi cardiac SPECT studies, the results were mixed. Wollenweber [9] and Chen [10] reported good correlation between CHO and human observer performance, but the CHO was not used to optimize reconstruction parameters in either of these studies. Narayanan [11] showed the good correlation between CHO and human observer performance for parameter optimization, but only if the images were grayscale instead of real-valued or if an observer internal noise model [14] was included in the CHO. Sankaran and Frey [12], [13] showed good correlation between the CHO and human observer performance for optimization of the filter cutoff frequency in post-reconstruction filtering, but did not compare the CHO and human performance in optimizing the number of iterations in their iterative reconstruction. The Sankaran and Frey studies did use grayscale images, but did not use internal noise in the CHO and used a very low lesion contrast (12.5%).

The study presented in this paper uses many of the same methods as the Sankaran and Frey studies, but explores some issues not addressed in those studies, including comparing the CHO and human observers for optimizing the number of iterations in reconstruction of the images. In this study, we increase the lesion contrast to a more clinically relevant level of 20%, but use the internal observer noise model to adjust the AUC values to a level that allows meaningful statistical analysis and comparison with human observer results. In addition, in this study we will use a more anatomically realistic phantom and simulate SPECT projection data with a more realistic Monte Carlo simulation as opposed to the analytical projection data simulation used by Frey [13]. Specifically, in this study, the CHO with the internal noise model will be compared to human observer performance for the optimization of the (number of subsets)/iteration and the number of iterations in the iterative ordered subset-expectation maximization (OS-EM) image reconstruction algorithm [15] used in obtaining the SPECT images.
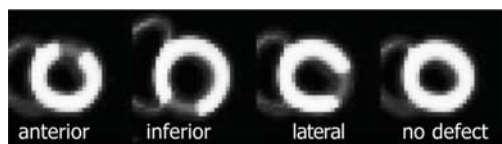
Fig. 1. Short axis slices of the heart of the NCAT phantom showing the defect size and locations. Contrast has been enhanced to 50% for display.

II. METHODS

A. Phantom

All the images used in this study were simulated using the 4D NURBs-based Cardiac Torso (NCAT) phantom [16]. The phantom modeled the uptake of ^{99m}Tc-sestamibi in the torso of a medium-large male patient who had lateral width of 37 cm and an anterior–posterior width of approximately 27 cm. The relative ^{99m}Tc-sestamibi organ uptake ratios per unit volume were 37.5, 37.5, 37.5, 2 and 1 for the heart, liver, kidneys, lung and background, respectively. The background is defined as all other parts of the torso not specifically listed above. The uptake in the liver relative to the heart, for this study, is considered high (on average the liver uptake is about half that of the heart for ^{99m}Tc-sestamibi), but still clinically realistic. The liver uptake was simulated at this high level to maximize the degrading effects of scatter from the liver into the myocardium and make the observer's task more difficult. Myocardial defects were simulated in the anterior, lateral, and inferior walls of the left ventricle (LV) myocardium. The size of the defects was 60° in the circumferential dimension and 2 cm in the longitudinal dimension. The defect contrast was 20% (uptake in defect was 80% of the normal wall uptake). The 20% defect contrast was chosen, based on previous discussions with physicians, because it is approximately the lowest contrast at which a physician would consider the LV to have a defect. Sample short-axis (SA) slices of the phantom through the LV myocardium are shown in Fig. 1 to show the size and location of the defects in the SA view.

B. Projection Data Simulation

The SPECT projection data were simulated using the SIMSET Monte Carlo code [17] and included the effects of nonuniform attenuation, collimator-detector response, and scatter. Very low noise projection data were simulated using a low-energy high resolution (LEHR) parallel collimator. The collimator had a hole-length of 3.5 cm, a hole-diameter of 1.5 mm, and septal thickness of 0.23 mm to yield an approximate spatial resolution of 1.1 cm FWHM at the center-of-rotation. The-radius of-rotation (distance from the center-of-rotation to the collimator face) was 22.5 cm. The detector modeled a sodium iodide crystal with a width of 50 cm $\times$ 50 cm and an intrinsic spatial resolution of 0.32 cm. Energy window was set at 140 keV $\pm 10\%$. The projection data were simulated into 128×128 bins (bin width $= 0.4$ cm) and 64 angles over 180° from the 45° left posterior oblique (LPO) view to the 45° right anterior oblique (RAO) view. The low noise data were then scaled to 64 000 myocardial counts for a 3.1 mm slice through the myocardium and Poisson noise was added. This count level is about $1/3$ that found in typical ^{99m}Tc-sestamibi clinical images and was set, based on results from preliminary studies,

so that the human observer study task would be of medium difficulty given the defect contrast of 20%.

C. Image Reconstruction and Processing

The SPECT images were reconstructed using the iterative OS-EM algorithm [15] with 10 different subset and iteration settings. The 10 settings were 1 and 4 (number of subsets)/iteration at 1, 3, 5, 7, and 9 iterations. The 1 subset/iteration resulted in 64 views/subset and is equivalent to the ML-EM algorithm. The 4 subsets/iteration resulted in 16 views/subset. The OS-EM reconstructions were performed with nonuniform attenuation correction only. After reconstruction, the images were reoriented to the short-axis (SA) view and a single slice, containing the defect centroid, was extracted. The SA images were then low-pass filtered with a Butterworth filter of order 5 and cutoff of 0.15 pixels^{-1}. These filter parameters were chosen based on previous work which found optimal filter parameters for similar simulated SPECT images [12], [13].

The SA images were then processed for the observer studies. First, a 32×32 pixel region containing the myocardium was extracted from each SA image. Next, the images were interpolated to 256×256 pixels using bilinear interpolation. Finally, the image pixel values were converted from real values to integer values ranging from 0 to 255. This processing is necessary for the human observer study display. For consistency, the CHO was applied to images processed in exactly the same way as the human observer study images. The CHO study used more images than the human observer study, but all the images used in the human observer study were also used in the CHO study.

D. Human Observer Study

In the human observer study, the observers were shown a series of images and asked to rate, on a discrete scale from 1 to 6, the likelihood that a defect was present in a given location in the LV wall. The location was indicated by a cross-hair, which the observers could toggle on and off. The displayed image size was approximately 10 cm $\times$ 10 cm for a single SA slice. The images were shown against a black background.

There were 5 human observers, all are researchers in SPECT imaging. For each observer, the study was split into two sessions, each session about 1 hour in length. Each session consisted of 5 blocks of images. Each block consisted of images reconstructed with a given parameter setting ([number of subsets]/iteration and number of iterations). Each block consisted of a training set of 48 images followed by a test set of 96 images. Within both the training and test sets, there was an equal number of defect-present and defect-absent images as well as an equal number of images for each of the three defect locations. The image order within each block was completely random. The order of the blocks was different for each observer and was designed to minimize reading order effects.

An ROC analysis and subsequent analysis of variance (ANOVA) of the human observer data were done using the jackknife method for multiple readers and multiple cases (MRMC) [18]. This analysis was performed with the LABMRMC [19] program which estimated the mean and standard deviation of the AUC for each parameter setting (i.e., treatment) and each observer and then performed the subsequent ANOVA. The

ANOVA tested the null hypothesis that the AUCs for the 10 parameter settings were equal. The results are generalizable to both similar cases and similar observers.

E. Channelized Hotelling Observer Study

The basic CHO paradigm used in this study is very similar to that used in the previous study by Frey [13]. The reader is referred to that study for a detailed description of the paradigm. This section details the specific parameters used in our CHO study.

The CHO model consisted of 3 radially-symmetric, square-profiled, non-overlapping channels with octave-based center frequencies and channel widths. The starting channel width and frequency were $1/64$ pixels $^{-1}$.

For each parameter setting, a separate CHO was calculated using a training set of 600 defect-present (3 defect locations $\times 200$ noise realizations) and 600 corresponding defect-absent images. Then, for each parameter setting, a collection of scalar rating values was obtained by taking the inner product of the 3-element CHO vector and each image vector in a "test" set. The test set was a similar but statistically-independent set of 600 defect-present and 600 defect-absent image vectors.

Since the collections of rating values were approximately Gaussian distributed, an estimated mean detectability, d_A, and corresponding variance, $\hat{\sigma}^2_{d_A}$, were calculated as given by Abbey *et al.* [3], using the following equations:

$$d_A = \frac{\hat{\mu}_{\lambda+} - \hat{\mu}_{\lambda-}}{\sqrt{\frac{1}{2}\left(\hat{\sigma}^2_{\lambda+} + \hat{\sigma}^2_{\lambda-}\right) + \hat{\sigma}^2_{\text{int}}}} \tag{1}$$

and

$$\sigma_{\hat{d}_A} = \frac{2}{\left(\hat{\sigma}^2_{\lambda+,\text{int}} + \hat{\sigma}^2_{\lambda-,\text{int}}\right)} \left[\frac{\hat{\sigma}^2_{\lambda+,\text{int}}}{N_+} + \frac{\hat{\sigma}^2_{\lambda-,\text{int}}}{N_-} \right.$$
$$\left. + \frac{(\hat{d}_A/2)^2}{\left(\left(\hat{\sigma}^2_{\lambda+,\text{int}} + \hat{\sigma}^2_{\lambda-,\text{int}}\right)\left(\frac{\hat{\sigma}^4_{\lambda+,\text{int}}}{N_+-1} + \frac{\hat{\sigma}^4_{\lambda-,\text{int}}}{N_--1}\right)\right)} \right] \tag{2}$$

where $\hat{\mu}_{\lambda+}$ and $\hat{\sigma}^2_{\lambda+}$ are the mean and variance of the rating values obtaining from the defect-present images, $\hat{\mu}_{\lambda-}$ and $\hat{\sigma}^2_{\lambda-}$ are the mean and variance of the rating values obtained from the defect-absent images, $\hat{\sigma}^2_{\text{int}}$ is the internal noise factor and N_+ and N_- are the number of defect-present and defect-absent images, respectively, and finally

$$\hat{\sigma}^2_{\lambda*,\text{int}} = \left(\hat{\sigma}^2_{\lambda*} + \hat{\sigma}^2_{\text{int}}\right). \tag{3}$$

The internal observer noise model, as given in equation (1), has been suggested and applied for model observers such as the CHO [3], [20], because it is known that human observers exhibit some randomness in rating images [14], [21]. There is no guide for how much internal noise to add in the absence of human observer results, so we tried many different levels of internal noise ranging from no noise to a level that was high enough to produce detectability values close to zero (AUCs close to 0.5) for all parameter settings. In this paper, the results will be presented at 3 values of internal noise: 0, 10, and 100.

For comparison with the human observer results, the d_A values were converted to AUC values using the following well-known relationship:

$$\text{AUC} = 0.5 + 0.5 * \text{erf}(d_A/2). \tag{4}$$

III. RESULTS

A. Human Observer Study

The estimated mean AUC values for the individual human observers are shown in Fig. 2 along with their corresponding 95% confidence intervals. Note the variation in the AUC values and trends among observers. At 1 and 3 updates, especially, there is a wide range in the absolute AUC values amoung observers. However, for all 5 observers the trend in AUC with an increasing number of updates has some similarities. The AUC tends to increase from 1 to 5 updates, reaches a maximum at 5 to 9 updates and then tends to decrease slightly from 9 to 36 updates. For all 5 human observers, the maximum mean AUC occurred at 1 subset and 5 to 9 iterations.

The MRMC ANOVA analysis tested the null hypothesis that the AUC was equal among the 10 parameter settings. The results of this analysis strongly rejected the null hypothesis with $p < 0.0001$. Thus, the ANOVA indicates that at least one of the parameter settings has a different AUC than the others, but the ANOVA does not tell us which one (or ones). Therefore, we performed a second MRMC ANOVA using only 8 of the parameter settings, specifically from 4 to 36 updates. For this analysis, the null hypothesis could not be rejected ($p = 0.1928$). Thus, for the range of 4 to 36 updates, the difference among the AUC values are not statistically significant. We can only say, with confidence, that the optimum parameter setting is neither 1 nor 3 updates.

B. Channelized Hotelling Observer Study

The estimated detectability (d_A) values obtained from the CHO are shown in Fig. 3, for 3 levels of internal noise. The errors bars on the mean d_A values show the corresponding 95% confidence intervals. For any two mean d_A values, if their 95% confidence intervals do not overlap, then difference between the two mean d_A values is statistically significant at the p=0.05 level. For all internal noise levels, the maximum mean d_A occured at 5 updates. The difference between the mean d_A at 5 updates and the mean d_A at 1, 3, 7, 9, 12, 29, 28, 36 updates is statistically significant at the p=0.05 level. The difference between the mean d_A at 5 updates and the mean d_A at 4 updates is *not* statistically significant at the p=0.05 level. Therefore, we can say with confidence, that the optimum OS-EM parameter setting, as determined by the CHO, is 4 or 5 updates.

The level of internal noise affected the absolute d_A values and the relative differences among the d_A values, but the not rankings of the d_A values. It is the rankings that determine the choice of an optimum parameter setting. Thus, regardless of the level of internal noise, the CHO predicted the optimal parameter setting to be either 4 updates (4 subsets and 1 iteration) or 5 updates (1 subset and 5 iterations).
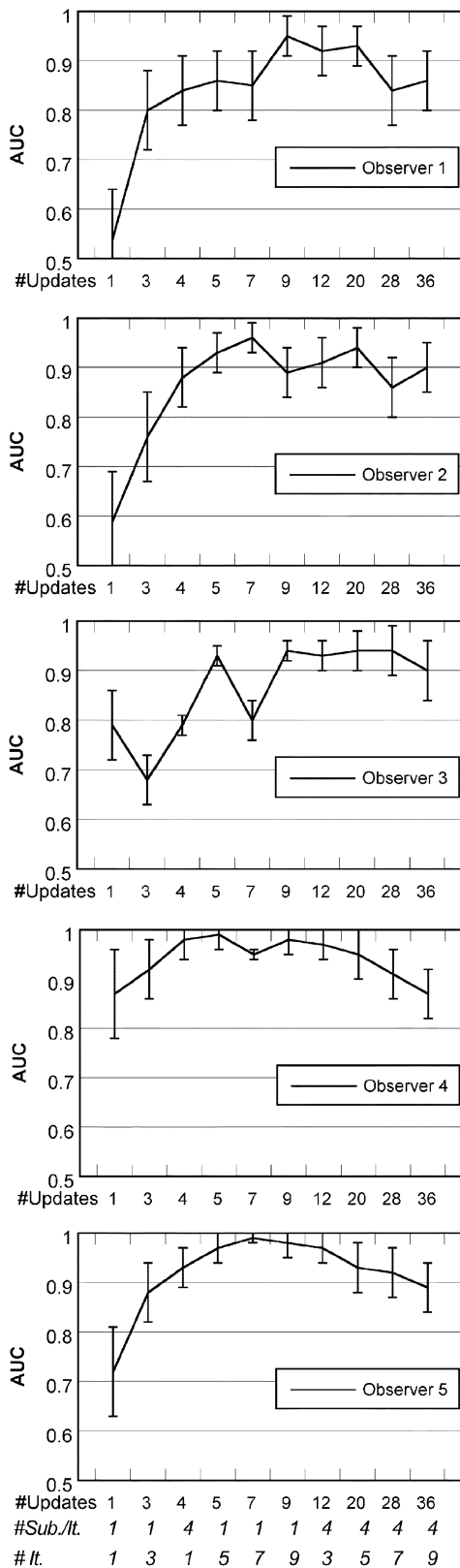
Fig. 2. Results from the human observer study. For each of the 5 human observers, the mean AUC values and corresponding 95% confidence intervals are shown for the OS-EM reconstruction parameters studied.
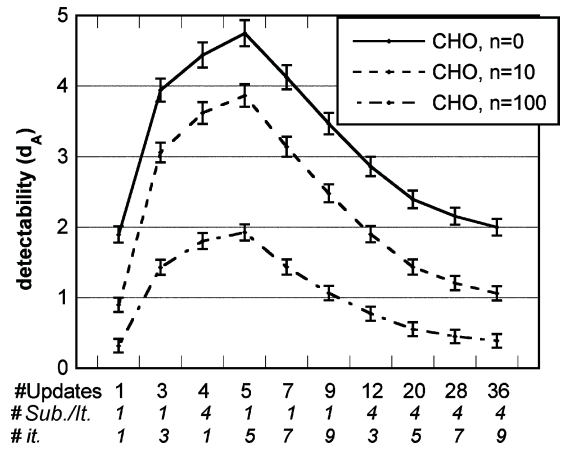

Fig. 3. Results from the CHO study. The detectability (d_A) values for the CHO at various levels of internal noise ($n = 0, 10$ & 100) for the OS-EM reconstruction parameters studied. Error bars for the CHO show 95% confidence intervals.
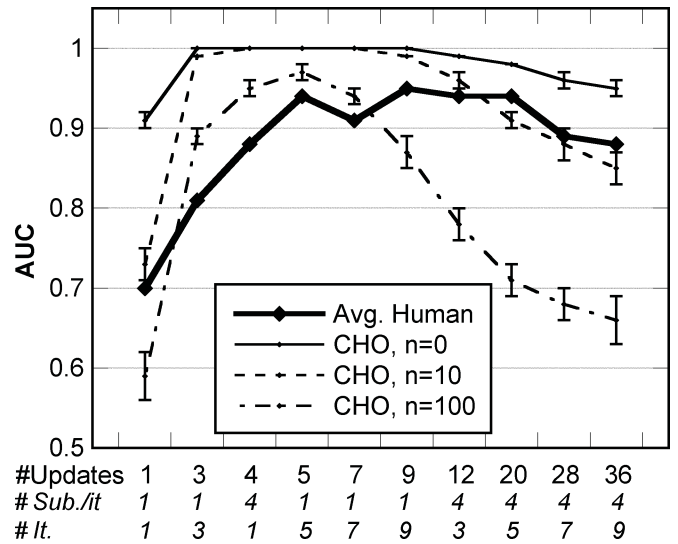

Fig. 4. The AUC values for the average of the human observers and for the CHO at various levels of internal noise ($n = 0, 10$ & 100) for the OS-EM reconstruction parameters studied. The AUC values for the CHO are calculated from the detectability values shown in Fig. 3. Error bars for the CHO show 95% confidence intervals.

The AUC values for the CHO (obtained from the d_A values shown in Fig. 3) are shown in Fig. 4 along with the mean AUC values averaged across all 5 human observers. The errors bars on the mean AUC values for the CHO and human studies show the 95% confidence intervals. Since the relationship between the d_A and the AUC is nonlinear, d_A values greater than approximately 3.6 translate to AUC values very close to 1; thus, the differences among the those AUC values and their corresponding 95% confidence intervals cannot be appreciated on the graph shown.

Fig. 4 shows that without the addition of internal noise, the AUCs for the CHO are much higher than for the human observers, indicating the task was much easier for the CHO than for the human observers. It is common in CHO studies for the CHO to give much higher absolute AUC values than the human observers [7]–[13].

IV. CONCLUSION AND DISCUSSION

The purpose of this study was to determine how well the CHO would predict human observer performance in determining op-

timum OS-EM reconstruction parameters for a ^{99m}Tc-sestmibi myocardial SPECT defect detection study. The CHO study predicted the optimum setting to be 4-5 updates, while the best we can conclude from the human study is that the optimum setting lies in a range of 4–36 updates. The CHO's optimum setting of 4–5 updates is within that range of optimum settings given by the human study. Furthermore, for any of the individual human observers, the maximum estimated mean AUC value occurred at either 5, 7, or 9 updates, which is very close that predicted by the CHO.

The inclusion of internal noise did not change the rankings of the CHO AUC values nor did it change the statistical significance of the differences among the AUC values. Thus, for parameter optimization studies, where one is only interested in the *rankings* of the detectability values, the level of internal noise does not appear to be important

The problem the CHO has in predicting human observer performance in this study is that the CHO does not predict the broad range of OS-EM reconstruction parameter values over which the mean AUC doesn't change much for the human observers. The graph in Fig. 3 shows a pronounced peak at 5 updates and shows the defect detection for the CHO to be fairly sensitive to the number of updates. However, the graph in Fig. 4 shows defect detection for the human observers to be much less sensitive to the number of updates. This result may be due to inadequate statistical power in the human observer study. The human observer study used 96 images per AUC estimate as compared to the CHO study which used 1,200 images per AUC estimate. However, it may also be that the CHO is too simple a model of human observers in some respects. Perhaps the CHO is too sensitive to changes in noise and resolution in the images as compared to individual observers, and perhaps the CHO needs to model or account for the variations among human observers at the task of defect detection. Further study of the CHO and its predictability of human observers is needed.

ACKNOWLEDGMENT

REFERENCES

[1] C.E. Metz, "ROC methodology in radiologic imaging," *Invest. Radiol.*, vol. 21, pp. 720–731, 1986.

[2] H. H. Barrett, J. Yao, J. P. Rolland, and K. J. Myers, "Model observers for the assessment of image quality," *Proc. National Academy Sci.*, vol. 90, pp. 9758–9765, 1993.

[3] C. K. Abbey, H. H. Barrett, and M. P. Eckstein, "Practical issues and methodology in assessment of image quality using model observers," *Proc SPIE*, vol. 3032, pp. 182–194, 1994.

[4] K. J. Myers, "Addition of a channel mechanism to the ideal observer model," *J. Opt. Soc. Amer. A*, vol. 4, pp. 2447–2457, 1987.

[5] W.E. Smith and H.H. Barrett, "Hotelling trace criterion as a figure of merit for the optimization of imaging systems," *J. Opt. Soc. Amer. A*, vol. 4, pp. 717–725, 1986.

[6] T. H. Farncombe, "Assessment of scatter compensation strategies for ^{67}Ga SPECT using numerical observers and human LROC studies," *J. Nucl. Med.*, vol. 45, pp. 802–812, 2004.

[7] T. H. Farncombe, "An optimization of reconstruction parameters and investigation into the impact of photon scatter in ^{67}Ga SPECT," *IEEE Trans. Nucl. Sci.*, vol. 49, no. 5, pp. 2148–2154, Oct. 2002.

[8] H. C. Gifford, R. G. Wells, and M. A. King, "A comparison of human observer LROC and numerical observer ROC for tumor detection in SPECT images," *IEEE Trans. Nucl. Sci.*, vol. 46, no. 4, pp. 1032–1037, Aug. 1999.

[9] S. D. Wollenweber, "Comparison of Hotelling observer models and human observers in defect detection from myocardial SPECT imaging," *IEEE Trans. Nucl. Sci.*, vol. 46, no. 6, pp. 2098–2103, Dec. 1999.

[10] M. Chen, "Observer studies of cardiac lesion detectability with triple-head 360° versus dual-head 180° SPECT acquisition using simulated projection data," *IEEE Trans. Nucl. Sci.*, vol. 49, no. 3, pp. 655–660, Jun. 2002.

[11] M.V. Narayanan, "Optimization of iterative reconstructions of ^{99m}Tc-sestamibi SPECT studies using numerical observers," *IEEE Trans. Nucl. Sci.*, vol. 49, no. 5, pp. 2355–2360, Oct. 2002.

[12] S. Sankaran, E. C. Frey, K. L. Gilland, and B. M. W. Tsui, "Optimum compensation method and filter cutoff frequency in myocardial SPECT: A human observer study," *J. Nucl. Med.*, vol. 43, pp. 432–438, 2002.

[13] E. C. Frey, K. L. Gilland, and B. M.W. Tsui, "Application of task-based measures of image quality to optimization and evaluation of three-dimensional reconstruction-based compensation methods in myocardial perfusion SPECT," *IEEE Trans. Med. Imaging*, vol. 21, no. 9, pp. 1040–1050, Sep. 2002.

[14] A. E. Burgess and B. Colbourne, "Visual signal detection IV. Observer inconsistency," *J. Opt. Soc. Amer. A, Opt. Image Sci.*, vol. 5, pp. 617–627, 1988.

[15] H. M. Hudson and R. S. Larkin, "Accelerated image reconstruction using ordered subsets of projection data," *IEEE Trans. Med. Image*, vol. 13, no. 4, pp. 601–609, Dec. 1994.

[16] W. P. Segars, "Development of a new dynamic NURBS-based cardiac-torso (NCAT) phantom," Ph.D. dissertation, Univ. North Carolina, Chapel Hill, May 2001.

[17] R. L. Harrison, "Preliminary experience with the photon history generator module of a public domain simulation system for emission tomography," *Conf. Rec. IEEE Nucl. Sci. Symp.*, pp. 1154–1158, 1993.

[18] D. D. Dorfman, K. S. Berbaum, and C. E. Metz, "Receiver operating characteristic rating analysis: Generalization to the population of readers and patients with the jackknife method," *Invest. Radiol.*, vol. 27, pp. 723–731, 1992.

[19] C. E. Metz, LABMRMC Analysis Software [Online]. Available: http://www.radio-logy.uchicago.edu/krl/roc_soft.htm

[20] A. C. Burgess, X. Li, and C.K. Abbey, "Visual signal detectability with two noise components: Anomalous masking effects," *J. Opt. Soc. Amer. A*, vol. 14, pp. 2420–2442, 1997.

[21] J. Qi, "Theoretical evaluation of the detectability of random defects in Bayesian emission reconstruction," In Information Processing in Medical Imaging, XVIIIth IPMI Int. Conf. (in (Lecture Notes in Computer Science)). Ambleside, New York, U.K., July 20–25, 2003, A. Goos, J Hartmanis, and J. van Leeuwen, Eds., Springer, pp. 354–365, 2003.